



## The limit analysis in soil and rock: a mature discipline of geomechanics\*

CHEN Zu-yu<sup>†</sup>

(China Institute of Water Resources and Hydropower Research, Beijing 100044, China)

(MOE Key Laboratory of Soft Soils and Geoenvironmental Engineering, Zhejiang University, Hangzhou 310027, China)

E-mail: chenzuyu@iwhr.com

Received Oct. 8, 2007; revision accepted Oct. 11, 2007

**Abstract:** The solution of a slope stability problem can be approached by its least upper-bound and maximum lower-bound with high accuracy. The limit equilibrium methods that employ vertical slices imply a lower bound of the factor of safety. It has been successfully extended to the area of active earth pressure analysis that accounts for different input of locations of earth pressure applications. Those methods that employ slices with inclined interfaces give an upper-bound approach to the stability analysis. It enjoys a sound mechanical background and is able to provide accurate solutions of soil plasticity. It has been successfully extended to the area of bearing capacity analysis in which various empirical coefficients are no longer necessary. The 3D upper- and lower-bound methods under this framework have been made possible and show great potential for solving various engineering problems.

**Key words:** Limit analysis, Geomechanics, Slope stability problem, Limit equilibrium method

**doi:**10.1631/jzus.2007.A1712

**Document code:** A

**CLC number:** TU3

### INTRODUCTION

The limit equilibrium method was developed almost simultaneously with the advent of the discipline of Soil Mechanics. By now it is still the major approach for geotechnical engineers to tangle with various practical problems. However, this method is more or less regarded as an empirical approach since some assumptions are to be introduced when the governing equations are set. Besides, it is considered as a well developed and understood method with no many demands for further updating.

As a branch of applied science, Soil Mechanics and Rock Mechanics benefit from the recent developments in the classic mechanics and computer science. The former provides a theoretical background, such as the upper-bound and lower-bound theorems of Plasticity, which enables us to establish a modern

system of limit analysis based on the traditional method of slices. The latter makes it possible to apply the theory to practical geotechnical problems.

In this paper, we will show that the limit equilibrium method is not as empirical as someone believes. New developments and findings also convince us that this is an area in which more research works will be needed.

### THEORETICAL FRAMEWORK

#### General

The framework of limit analysis using the upper-bound and lower-bound theorems, as applied for Soil Mechanics, was established by Chen (1975). However, his work is limited to analytical approaches that can hardly be extended to practical problems in which the complicated geometry of slope profiles always exclude any possibilities for analytical solutions. The statements described in this Section try to formulate the basic principles of Plasticity by an ap-

\* The Zeng Guo-Xi Lecture, May 22, 2007; Project (Nos. 50539100, 50679035 and 50509027) supported by the National Natural Science Foundation of China

<sup>†</sup>Academician of Chinese Academy of Sciences

proximation that discretizes the failure mass by slices in 2D areas, or columns in 3D areas. This is an approach that has been successfully applied to geotechnical engineering to deal with practical problems during the past half century.

Another approach commonly adopted in geotechnical engineering is factor of safety  $F$ , which reduces the available shear strength criteria to bring the structure to a state of limiting equilibrium by the following equations:

$$c_e = c/F, \tag{1}$$

$$\tan \phi_e = \tan \phi/F, \tag{2}$$

where  $c$  and  $\phi$  are cohesion and friction angle respectively. In the following presentations, the subscript ‘ $e$ ’ appeared for all variables invariably means that the related  $c$  and  $\phi$  values are reduced by Eqs.(1) and (2). The factor of safety  $F$  always keeps a monotonic relationship with the loading factor  $\eta$  used in Plasticity, although a formal demonstration is not available. Therefore the theoretical statements regarding the upper- and lower-bounds in this paper based on the ultimate load can be extended to the factor of safety approach.

In the establishment of the limit analysis framework, a ‘true failure mechanism’ is assumed. It is symbolized by a slip surface  $\Gamma$  that separates the soil body into two domains: the plastic sliding mass  $\Omega$  and the elastic zone  $E$ , which overlay and underlay the slip surface respectively under the application of an ultimate load  $T$  (Figs.1 and 3). Detailed description will be given as follows.

**Statements for the lower-bound approaches**

1. Theoretical statements

The lower-bound method as applied in slope stability analysis can be stated as follows.

Assume that a true failure mechanism as shown in Fig.1 exists with an associated ultimate load  $T$ , then, any external load  $T^0$  that balances a statically admis-

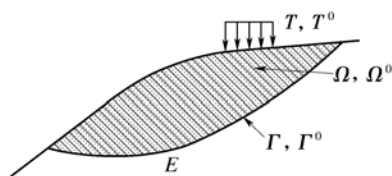


Fig.1 The lower-bound method as applied for slope stability analyses

sible stress field  $\sigma_{i,j}^0$  on  $\Omega$  and  $\Gamma$  will be smaller than or equal to  $T$ .

By ‘statically admissible stress field’, we mean that  $\sigma_{i,j}^0$  follows the equilibrium condition

$$\sigma_{i,j}^0 = W_i, \tag{3}$$

under the restrictions for physical admissibility that require:

(1) No shear failure develops, i.e.,

$$\tau - \sigma_n \tan \phi - c \leq 0; \tag{4}$$

(2) No tension develops, i.e.,

$$\sigma_3^0 \leq 0, \tag{5}$$

where  $W_i$  is the external load,  $\sigma_n$  and  $\tau$  are normal and shear strength on the failure surface, and  $\sigma_3^0$  is the minor principal stress.

2. The generalized method of vertical slices

As a simplified approach, our profession has a long history of employing the method of vertical slices to solve various practical problems of geotechnical engineering based on the lower-bound theoretical background. The method proposed by Morgenstern and Price (1965), as well as by others (Bishop, 1955; Janbu, 1973), implies a lower-bound approach with the following formulations.

(1) To allow the satisfaction of Eq.(3) for each slice, the force and moment equilibrium equations are established as (Chen and Morgenstern, 1983):

$$\frac{dG}{dx} - \tan \psi \frac{d\beta}{dx} G = -p(x) \sec \psi, \tag{6}$$

$$G \sin \beta = -y \frac{d}{dx} (G \cos \beta) + \frac{d}{dx} (y_i G \cos \beta) + \eta \frac{dW}{dx} h_i, \tag{7}$$

where

$$p(x) = \frac{dW}{dx} \sin(\phi_e - \alpha) + q \sin(\phi_e - \alpha) + c_e \sec \alpha \cos \phi_e - r_u \frac{dW}{dx} \sec \alpha \sin \phi_e + \eta \frac{dW}{dx} \cos(\phi_e - \alpha), \tag{8}$$

$$\psi = \phi_e - \alpha + \beta, \tag{9}$$

$G$ =the total interslice force;  $y_i$ = $y$  value of the point of



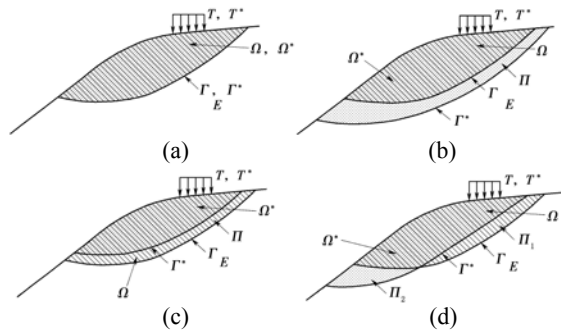


**Fig.3 The upper-bound method as applied for slope stability analyses. (a) The true failure mechanism  $\Omega$  and  $\Gamma$  completely overlaps the postulated one  $\Omega^*$  and  $\Gamma^*$ ; (b)  $\Omega$  and  $\Gamma$  are completely inside  $\Omega^*$  and  $\Gamma^*$ ; (c)  $\Omega$  and  $\Gamma$  are completely outside  $\Omega^*$  and  $\Gamma^*$ ; (d)  $\Gamma$  intersects  $\Gamma^*$**

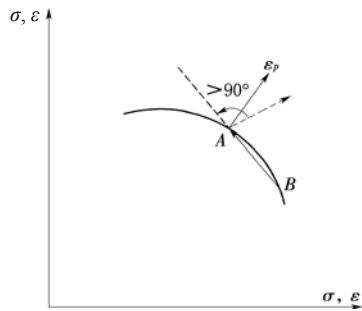


**Fig.4 Determining  $\epsilon_{ij}^*$ ,  $u^*$  and  $\sigma_{ij}^*$  based on the normality flow law**

inclined slices to solve various practical problems of geotechnical engineering. This method is based on the Mohr-Coulomb associated flow law that makes the procedures of solving equation much easy as follows.

(1) As an approximation to  $\Omega^*$ , divide the failure mass into a number of inclined slices, as shown in Fig.5. Here, the inclined interfaces are regarded as a part of slip surface  $\Gamma^*$  and the slice itself is assumed to be rigid block in which no energy dissipation develops.

(2) The Mohr-Coulomb associated flow law based on the equality part of Eq.(4) requires (Fig.6a):

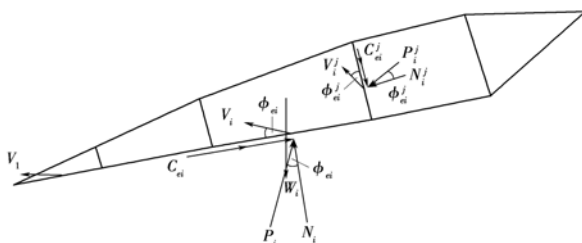


**Fig.5 The upper-bound method as applied for slope stability analysis**

$$\frac{V_n}{V_s} = \frac{\partial f / \partial \sigma}{\partial f / \partial \tau} = -\tan \phi_e, \quad (13)$$

where  $V_n$  and  $V_s$  are normal and tangential velocities respectively.  $\tau$  and  $\sigma$  are shear and normal stresses respectively.  $\phi_e$  is the reduced friction angle as defined by Eqs.(1) and (2). This means that the plastic velocity developed by an increment of external load should incline at a friction angle to the failure surface.

(3) The internal energy dissipation by the total stresses of the failure surface can be expressed as

$$D = (\tau V_s + \sigma V_n)A = (\tau \cos \phi_e + \sigma \sin \phi_e)VA = (c \cos \phi_e - u \sin \phi_e)VA, \quad (14)$$

where  $A$  is the area of the failure surface and  $V$  is the magnitude of the velocity.

As shown in Eq.(14), the advantage of adopting Mohr-Coulomb associated flow rule is that the energy dissipation can be determined without the knowledge of the internal stresses, which are generally unknown. This can be illustrated by Fig.6b in which the resultant of the normal effective force  $N$  and the shear resistance contributed by friction, designated  $P$ , inclines at an angle of  $\phi_e$ . Therefore  $P$  is perpendicular to  $V$  and does not work when Eq.(14) is established.

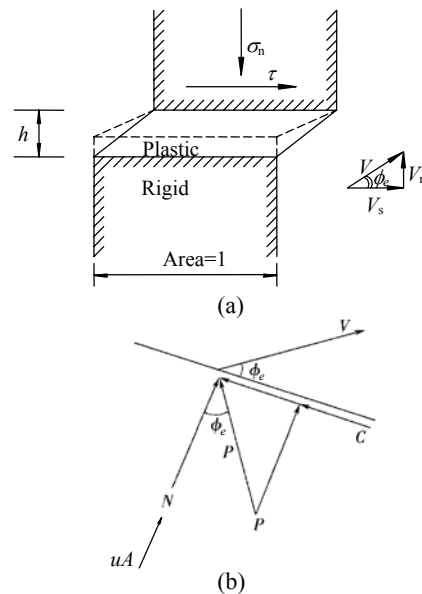


**Fig.6 The plastic velocity that inclines at an angle of  $\phi_e$  to the failure surface (a) The plastic velocities; (b) The 'combined frictional force'**

While Fig.3 is simplified to Fig.5, Eq.(12) in the upper-bound approach is approximated as

$$\sum_{k=1}^{n-1} D_{ek}^j + \sum_{i=1}^n \Delta D_{ei}^s = WW^*, \quad (15)$$

where the two terms in the left-hand side of Eq.(15) represent the internal energy dissipations developed on the interfaces and slip surface respectively, and determined by Eq.(14). Eq.(15) adopts the factor of safety that involved in the subscript 'e'. The external load  $T$  in Eq.(15) no longer exists.

(4) The true failure mechanism is determined by searching the minimum value of  $F$  associated with a critical discretization pattern.

The slip surface is discretized into a number of nodal points that are connected by either smooth curves or straight lines designated  $A_1, A_2, \dots, A_6$  (Fig.7). The inclinations of the interfaces are designated as  $\delta_1, \delta_2, \dots, \delta_6$ , associated with  $B_1, B_2, \dots, B_6$ . The optimization method will find these variables that give the minimum factor of safety. A great number of literatures (Chen and Shao, 1988; Chen, 1992; Chen *et al.*, 2001b) have dealt with this subject. Although most of them are concerned with the method of vertical slices, the algorithms equally apply to the method of inclined slices.

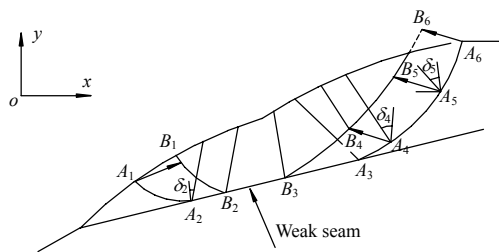


Fig.7 The optimization process for locating the critical failure mode

Donald and Chen (1997) demonstrated that the upper-bound method is identical with the Sarma (1979)'s method that employs force equilibrium approaches with rather complicated mathematical formulations. Also, the optimization process was not included in this method.

## SLOPE STABILITY ANALYSES BASED ON THE METHOD OF SLICES

### Formulations for the generalized methods of slices

#### 1. Solutions to the governing equations

Chen and Morgenstern (1983) gave the solutions to Eqs.(6) and (7), which are subsequently extended by Chen and Li (1998) to incorporate active earth pressure problems. The solutions to the force and moment requirements of Eqs.(6) and (7) are:

$$\int_a^b p(x)s(x)dx = G_m, \quad (16)$$

$$\int_a^b p(x)s(x)t(x)dx = M_m, \quad (17)$$

where

$$s(x) = \sec \psi E(x), \quad (18)$$

$$E(x) = \exp \left[ -\int_a^x \tan \psi \frac{d\beta}{d\xi} d\xi \right], \quad (19)$$

$$t(x) = \int_a^x (\sin \beta - \cos \beta \tan \alpha) E^{-1}(\xi) d\xi, \quad (20)$$

$$G_m = P_w - PE(b), \quad (21)$$

$$M_m = P_w h_w - P[h \cos \delta + t(b)E(b)] + \int_a^b \eta_i \frac{dW}{dx} h_i dx, \quad (22)$$

where  $P$  is the value of  $G(x)$  at  $x=b$ , or active earth pressure at the vertical wall;  $P_w$  is the water pressure at  $x=a$ , i.e.  $P_w=G(a)$ ;  $h$  is the distance between the point of application of the active earth pressure and the bottom of the wall, i.e., the value of  $(y-y_i)$  at  $x=b$ ;  $h_w$  is the distance between the point of application of the water pressure and the bottom of the tension crack, i.e., the value of  $(y-y_i)$  at  $x=a$ ;  $\delta$  is the value of  $\beta$  at  $x=b$ , i.e., the friction angle at the wall in case of earth pressure problems.

#### 2. Solving for $F$ and $\lambda$

Eqs.(16) and (17) involve an unknown  $F$  (or  $P$ ) and an unknown variable  $\beta(x)$ . Chen and Morgenstern (1983) suggested introducing an assumption defining  $\beta(x)$ :

$$\tan \beta = f_0(x) + \lambda f(x), \quad (23)$$

where  $f(x)$  is a linear function that allows the value  $f_0(a)$  and  $f_0(b)$  to be equal to the values of  $\tan \beta$  at  $x=a$  and  $x=b$  respectively.  $f_0(x)$  is another function that has zero values at  $x=a$  and  $x=b$ . Criteria of fixing the boundary values of  $\tan \beta$  at  $x=a$  and  $x=b$  have been given to ensure satisfaction of the principal of complementary shear stresses (Chen and Morgenstern, 1983).

In practical applications, the following two approaches are normally used.

**Assumption 1** Takes  $f_0(x)=0$  and  $f(x)=1$  (Fig.3b). This means that  $\tan\beta$  is a constant  $\lambda$ . This method is normally referred to as Spencer (1966)'s method.

**Assumption 2** Takes  $f_0(x)$  as a linear function and  $f(x)$  as a sine function (Fig.3c). This approach is particularly useful when active earth pressure  $P$  is determined.

It is possible to find  $F$  (or  $P$ ) and  $\lambda$  from Eqs.(16) and (17) by iterations. For details refer to Chen and Morgenstern (1983) or Chen and Li (1998).

**Formulations for the upper-bound method**

1. Solutions to the velocity field

For a pair of adjacent slices, the velocity of the left and right slices  $V_l, V_r$  and the relative velocity  $V_j$  form a closed triangle. Therefore we have (Fig.8)

$$V_r = V_l \sin(\theta_l - \theta_j) / \sin(\theta_r - \theta_j), \tag{24}$$

$$V_j = V_l \sin(\theta_r - \theta_l) / \sin(\theta_r - \theta_j), \tag{25}$$

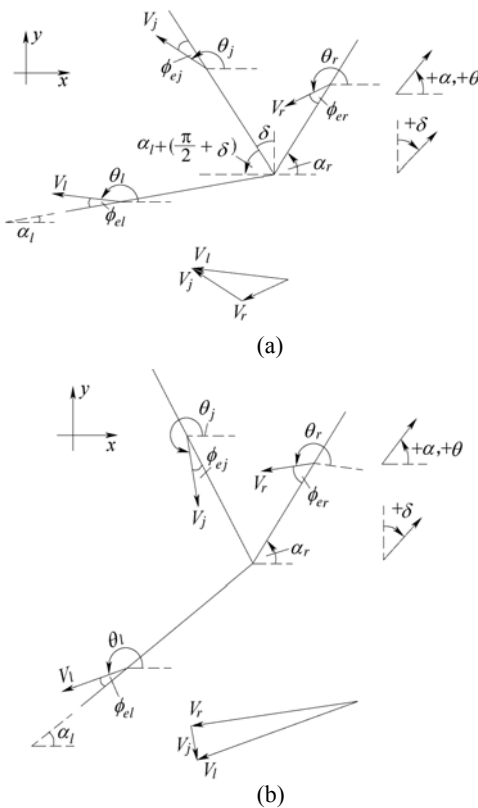


**Fig.8 Determining  $V_r$  and  $V_j$  based on  $V_l$**   
 (a) The left slice moves upward relative to the right one;  
 (b) The left slice moves downward relative to the right one

where  $\theta$  is the angle of the velocity vector measured from the positive  $x$  axis. Donald and Chen (1997) argued that there are two possible directions of relative movement: the left slice moves upward relative to the right one as shown in Fig.8a or downward as shown in Fig.8b.

For a slice numbered  $i$ ,  $V_l, V_r$  and  $V_j$  can be expressed as a linear function of the velocity of the left first slice  $V_1$  (Fig.5):

$$V_i = \kappa V_1, \tag{26}$$

where

$$\kappa = \prod_{j=1}^i [\sin(\alpha_i^l - \phi_{ei}^l - \theta_i^l) / \sin(\alpha_i^r - \phi_{ei}^r - \theta_i^r)], \tag{27}$$

$l$  and  $r$  refer to the left and right sides of the interfaces.

Eq.(24) can be transformed to an integral if the width of the slice approaches to infinitesimally small (Fig.9),

$$V = \kappa \exp \left[ - \int_{x_0}^x \cot(\alpha - \phi_e - \theta_j) \frac{d\alpha}{d\zeta} d\zeta \right] V_1, \tag{28}$$

and Eq.(25) yields

$$V_j = -V_0 \csc(\alpha - \phi_e - \theta_j) E(x) d\alpha. \tag{29}$$

2. Solving for  $F$

Substituting Eqs.(28) and (29), Eq.(15) becomes

$$\int_{x_0}^{x_n} \left[ (c_e \cos \phi_e - u \sin \phi_e) \sec \alpha - \frac{dW}{dx} \sin(\alpha - \phi_e) \right] E(x) dx - \int_{x_0}^{x_n} (c_e^j \cos \phi_e^j - u^j \sin \phi_e^j) L \csc(\alpha - \phi_e - \theta_j) \frac{d\alpha}{dx} E(x) dx + K_i = 0, \tag{30}$$

where  $K_i$  is a coefficient accounting for possible discontinuities in  $\alpha$  and  $\phi_e$ :

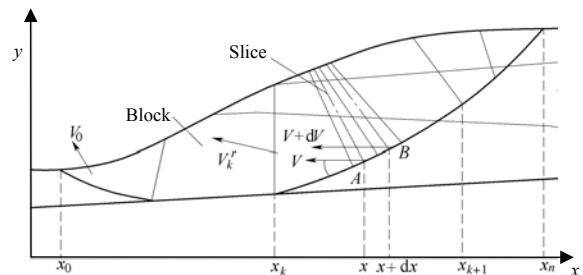


**Fig.9 Determining  $V_r$  and  $V_j$  by integration**

$$K_i = -\sum_{i=1}^n [(c_e^j \cos \phi_e^j - u^j \sin \phi_e^j)_i L_i \csc(\alpha^r - \phi_e^r - \theta_j) \cdot \sin(\Delta\alpha - \Delta\phi_e)_i E^l(x_i)]. \quad (31)$$

The subscript ‘e’ involved in the variables implies an unknown value of factor of safety  $F$  by the definition of Eqs.(1) and (2).

**Validation and illustrative examples**

The two examples shown in this Section are mainly aimed at validating the upper-bound method, compared to the method of vertical slices, which is original in the discipline of Soil Mechanics.

**Example 1** Comparisons among various methods

Figs.10 and 11 show a test example that is taken from (Donald and Giam, 1992). The geometric details and geotechnical property parameters can be found in Donald and Giam (1992).

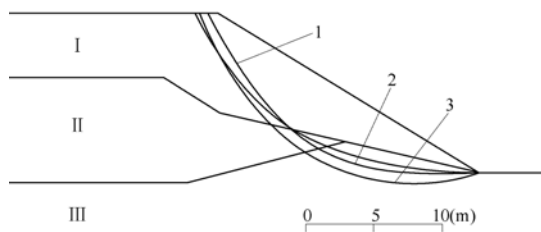


**Fig.10** Comparisons of the critical slip surfaces obtained from various methods. 1: Spencer,  $F=1.366$ ; 2: Bishop,  $F=1.378$ ; 3: Upper-bound,  $F=1.401$

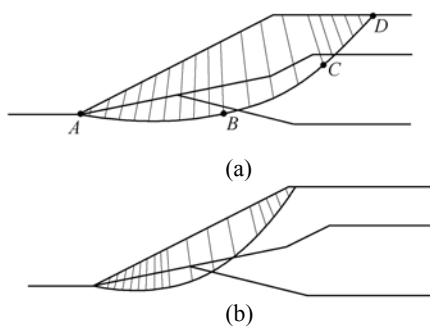


**Fig.11** The upper-bound solutions for Example 1  
(a) The initial failure mode; (b) The critical one

The slip surface is defined by 4 nodal points designated as  $A, B, C, D$  connected by smooth curves as shown in Fig.11a. The slip surfaces 1 and 2 in Fig.10 are related to the methods of Spencer ( $F=1.366$ ) and Bishop ( $F=1.378$ ) respectively. Fig.11 shows the calculation details using the upper-bound method.

The factor of safety for the initial failure mode using Eq.(30) was 1.630 as shown in Fig.11a. The minimum  $F$  for the critical failure mode shown in Fig.11b was 1.401. The critical failure surface, designated 3 in Fig.10, can be compared with those given by the conventional methods designated 1 and 2.

**Example 2** An uniform slope subjected to a vertical surface load

For a uniform slope subjected to a vertical surface load, Sokolovski (1960) gave a closed-form solution with the assumption that the weight of the soil is neglected. The plastic zone is shown in Fig.12. The slip surface consists of two straight lines and a log-spiral. The ultimate load  $q$  is determined by

$$q = c \cot \phi \left[ \frac{1 + \sin \phi}{1 - \sin \phi} \exp[(\pi - 2\gamma') \tan \phi] - 1 \right], \quad (32)$$

where  $\gamma'$  is the sloping angle of the surface line.

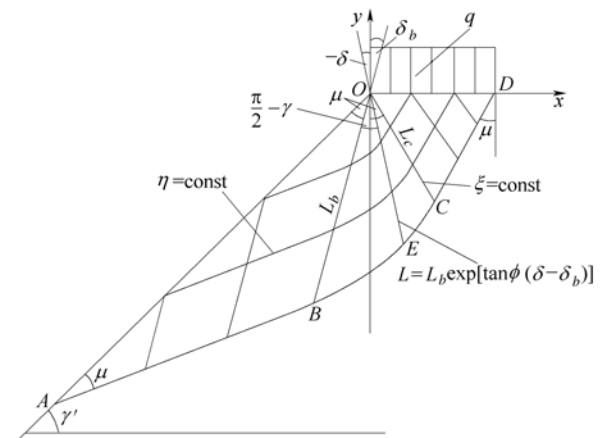


**Fig.12** A uniform slope subjected to a vertical surface load (Sokolovski, 1960)

It has been demonstrated that with this particular slip surface, Eq.(30) is reducible to Eq.(32). Details are given by Chen *et al.*(2005).

The numerical work adopts  $c=98$  kPa,  $\phi=30^\circ$ , and the closed-form solution for the ultimate load  $q$  is 111.44 kPa. Associated with this load, we started with a 4-block mechanism as shown in Fig.13a. Using the upper-bound method, it is easy to find that the value of factor of safety is  $F=1.047$  by Eq.(30). The optimization procedures described in Fig.7 gave a critical failure mode as shown in Fig.13b with a solution  $F_m=1.013$ . As the failure mass was divided into 16 slices, we obtained a failure mode almost identical to

the one suggested by the closed-form solution as shown in Fig.12c, associated with  $F_m=1.006$ .

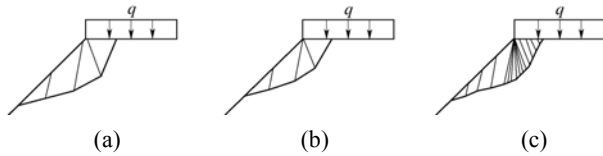


**Fig.13** Calculations by the upper-bound method for Example 2

(a) The initial failure mode with 4 blocks; (b) The critical failure mode with 4 blocks; (c) The critical failure mode with 16 blocks

## FROM SLOPE STABILITY TO EARTH PRESSURE ANALYSES

### General

The active earth pressure is normally determined by Coulomb's theory that considers a straight line slip surface and force equilibrium condition only. This approach also implies an assumption that the point of earth pressure application is located at the lower one-third of the wall. These assumptions limit the Coulomb's theory to be used only in gravity types of walls. In other words, it is assumed that the earth pressure applied to the wall is distributed in a triangle shape. In the ASCE Conference in memory of 50 years experience for earth pressure, Peck (1992) wrote that:

*Now we understand that the distribution of the pressure is related to the deformation conditions, and we appreciate that the significance of these conditions was indeed the outstanding contribution of Terzaghi in his cigar box tests at Robert College and his large scale tests at MIT, ..., where he demonstrated that various deformation conditions could lead to a center of pressure anywhere between lower and upper third points.*

The generalized method of slices presented in this paper considers moment equilibrium condition and covers the boundary condition of an external load  $P$  at the end  $x=b$ . This method thus permits the slope stability analysis method to be extended to earth pressure problems with varied location of point application. On the other hand, this generalized method can be used to validate the empirical coefficients used

for calculating the active earth pressure on a flexible wall where Coulomb's theory is not applicable. An illustrative example is presented here. Further studies regarding comparisons between the results calculated by Terzaghi–Peck–Mesri empirical method and analytical approaches can be found in Chen and Li (1998).

### An illustrative example

**Example 3** Calculating the active earth pressures with different input of  $k$

Fig.14a shows a 12 m high retaining structure backfilled with a cohesionless soil with  $\phi=36^\circ$ . The unit weight of the material is  $\gamma=20.58 \text{ kN/m}^3$ . The classical active earth pressure per meter width can be calculated as

$$P_a = \tan^2(45 - \phi/2)\gamma H^2 / 2 = 384.7 \text{ kN}.$$

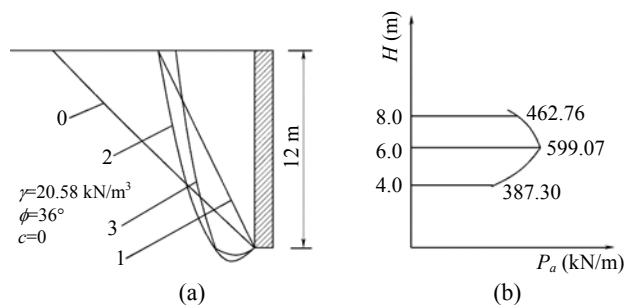


**Fig.14** Calculating the active earth pressures with different input of  $k$ . (a) The initial critical slip surfaces; (b) The active earth pressures

Fig.14a shows the critical slip surfaces associated with different locations of points of application starting from the same initial slip surface numbered 0. Defining  $k=h/H$ , the calculated slip surfaces 1, 2, 3 correspond to the cases  $k=1/3, 1/2, 2/3$  associated with  $P_a=387.3, 599.1$  and  $462.8 \text{ kN}$  respectively. The active pressure obtained for the case  $k=1/3$  was very close to the classical solution. The associated critical slip surface (curve 1) was almost a straight line, while those for case  $k=1/2$  or  $k=2/3$  (curves 2 and 3) exhibited a rather curved shape. The results are in general agreement with the understanding that a supported wall, such as the braced, anchored or cantilever wall, which has a  $k$  value close to  $1/2$ , usually presents a larger active earth pressure, compared with that of a gravity wall.

FROM SLOPE STABILITY TO BEARING CAPACITY ANALYSES

General

The traditional bearing capacity analysis method adopts Prandtl solution that is based on the slip-line field method. Sokolovski (1960) provided a comprehensive review of this method and a number of solutions to bearing capacity problems. However, since this method employs purely analytical approaches, it is practically impossible to handle geotechnical problems that normally have complicated geometry and material properties. The Prandtl solution is thus attached by a number of empirical coefficients accounting for the influence of the weight of soils, embedment of footings, inclination of the surface load, etc. These treatments are still insufficient if the foundation is layered, irregularly shaped, and partly submerged by ground water.

The upper-bound method described in this paper has a sound theoretical background. Example 2 shows that this method is able to produce the results identical to those provided by slip-line field theory. Therefore, various empirical coefficients are no longer necessary.

On the other hand, this method can also be used to evaluate the feasibility of various empirical coefficients currently being used. Detailed discussions can be found in Wang *et al.*(2001). An illustrative example is presented here.

An illustrative example

**Example 4** Calculating the bearing capacity for a uniform foundation

To demonstrate the accuracy of the upper-bound method applied to bearing capacity analysis, let us review a simple problem that involves a uniform soil foundation under a vertical surface load. For a weightless and cohesionless soil foundation, as shown in Fig.15, with the parameters  $c=30 \text{ kN/m}^2$  and  $B=17 \text{ m}$ , the well-known Prandtl solution gives. The initial failure mode is randomly defined by 5 nodal points connected by a smooth curve and 4 inclined interfaces. The factor of safety calculated by Eq.(30) is 1.704. The optimization process gives a critical failure mode as show in Fig.15b associated with a minimum factor of safety  $F=1.004$ . It can be found that not only the value of  $F$  meets the theoretical answer but also the failure mode depicts a slip line field almost identical to the closed-form solution.

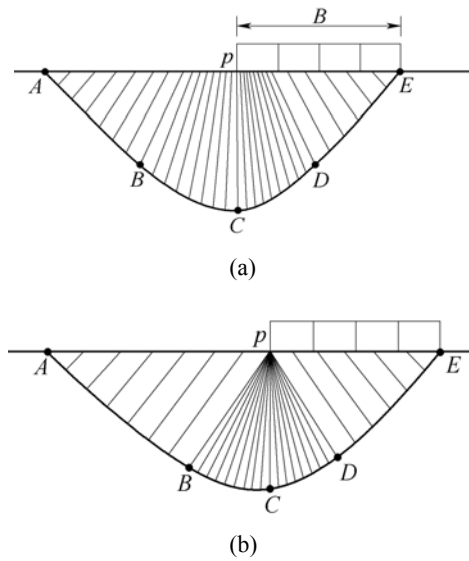


Fig.15 Calculating the bearing capacity for a uniform foundation

(a) The initial failure mode; (b) The critical failure mode

FROM 2D TO 3D ANALYSES

General

To-date, applications of the limit equilibrium method have been mainly limited to 2D area, although its potential to 3D area is great (Seed *et al.*, 1990; Morgenstern, 1992). Duncan (1996) summarized the main research outcomes of the development of 3D analysis methods during the past 25 years since 1966.

In the 3D area, the failure mass is divided into a series of columns (Fig.16), either with vertical inter-column faces in the limit equilibrium approaches, or inclined faces in the upper-bound method.

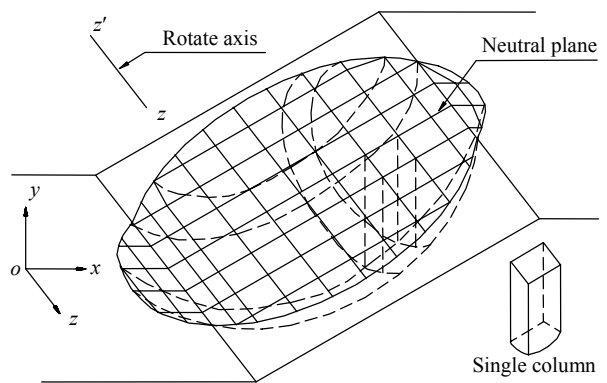


Fig.16 3D slope stability analysis using the 'method of columns'

It has been shown that in the 2D area any limit equilibrium (lower-bound) method involves some assumptions regarding the inter-slice forces in order to render the problem statically determinate. Extending the limit equilibrium method to 3D areas encounters even more serious challenges on all these limitations. One method differs from the others in terms of: (1) the assumptions made on the inter-column forces; (2) the equations that render mechanical equilibrium conditions; and (3) simplifications regarding the shape of the slip surfaces.

On the other hand, the upper-bound method described has also been extended into 3D areas. While it enjoys more rigorous theoretical background, the optimization procedures in finding the critical failure mode can be challenging due to the increasing number of freedoms in the 3D areas.

This Section briefly reviews the recent developments in this area by the author's research group.

**The limit equilibrium approach—3D Spencer method**

Chen *et al.*(2003) made the following three assumptions:

(1) The horizontal shear forces on the row-interfaces (*ABFE* and *DCGH* in Fig.17) are neglected, i.e., the inclination of inter-column force *G* to the *x*-axis, designated  $\beta$ , is assumed to be parallel to the *xoy* plane. It is further assumed that  $\beta$  is constant for all columns.

(2) Shear forces applied to the column-interfaces (*ADHE* and *BCGF* in Fig.17) are neglected.

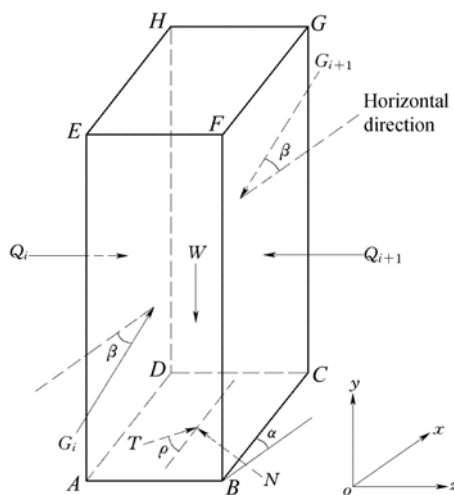


Fig.17 Assumptions made for the internal forces (Chen *et al.*, 2003)

(3) The shear force applied to any column base *T*, is assumed to be inclined at an angle of  $\rho$  measured from *xoy* plane to the positive *z*-axis. For prisms in any column direction (i.e., those with constant *z* values),  $\rho$  is taken to be constant. In the *z*-direction,  $\rho$  is defined as (Fig.18),

$$\begin{aligned} \rho_R &= \kappa \cdot z, & z < 0; \\ \rho_L &= -\eta\kappa \cdot z, & z \geq 0. \end{aligned} \tag{33}$$

This means that the basal shear forces on the left and right sides of the central *xoy* plane take opposite directions and vary linearly with respect to the *z*-axis.

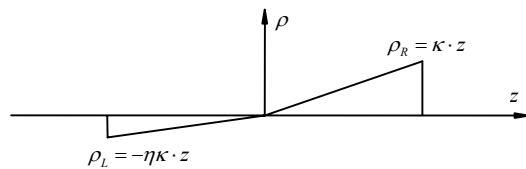


Fig.18 Assumptions made for the distribution of  $\rho$

By projecting all of the forces to a column in the direction *S'* that is perpendicular to the inter-column forces *G* (Fig.19), a straight forward equation calculating the normal force *N<sub>i</sub>*, applied on the column base can be obtained:

$$N_i = \frac{W_i \cos \beta + (uA_i \tan \phi'_e - c'_i A_i)(-m_x \sin \beta + m_y \cos \beta)}{-n_x \sin \beta + n_y \cos \beta + \tan \phi'_e (-m_x \sin \beta + m_y \cos \beta)} \tag{34}$$

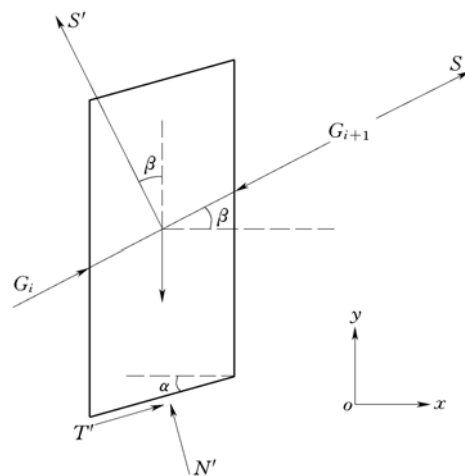


Fig.19 Projecting all of the forces on a column in the direction *S'*

where  $u$  is the pore pressure at the column base (of area  $A_i$ ).  $W_i$  is the weight of the column.  $m_x, m_y, m_z$  are direction cosines of the shear force  $T$ , and  $n_x, n_y, n_z$  are direction cosines of the normal to the column base.

Establishing the force equilibrium equations in  $y$  and  $z$  directions and the moment equilibrium equation around  $z$ -axis, the method obtained the following three controlling equations:

$$S = \sum [N_i(n_x \cos \beta + n_y \sin \beta)_i + T_i(m_x \cos \beta + m_y \sin \beta)_i - W_i \sin \beta] = 0, \quad (35)$$

$$Z = \sum (N_i \cdot n_z + T_i \cdot m_z) = 0, \quad (36)$$

$$M = \sum [-W_i x - N_i n_x y + N_i n_y x - T_i m_x y + T_i m_y x] = 0, \quad (37)$$

which involves three unknowns  $F, \beta$  and  $\kappa$  to be solved by the Newton-Raphson method.

This method allows satisfaction of complete overall force equilibrium conditions and the moment equilibrium requirement about the main axis of rotation. The computational procedure is simple because it involves only three unknowns.

### The 3D upper-bound analysis

The 3D upper-bound method divides the failure mass into a series of columns with inclined interfaces. Using the symbol  $\Downarrow$  to represent the interfaces between two adjacent columns, and  $\leftrightarrow$ , between two adjacent rows of prisms, the 3D work-energy balance equation, extended from Eq.(15) is

$$\sum D_{i \leftrightarrow j, e}^* + \sum D_{i \Downarrow j, e}^* + \sum D_{i, j, e}^* = \mathbf{WV}^*. \quad (38)$$

The three terms in the left-hand side of Eq.(38) represent the energy dissipations developed on the row-to-row, column-to-column and the basal surfaces of a prism respectively. The postulated failure mechanism is represented by a superscript  $^*$ .

The right side of Eq.(38) sums up the work done by  $\mathbf{W}$ , the weight of the prism.  $\mathbf{V}$  is the velocity developed by a small increment of the external load.

By employing the Mohr-Coulomb associated flow law and conditions for kinematical compatibility, we have the following relationships:

(1) The plastic velocity is inclined at an angle of  $\phi_e$  to the failure plane, i.e.

$$\Phi(\mathbf{V}, \mathbf{N}) = \cos(\pi/2 - \phi_e) = \sin \phi_e, \quad (39)$$

where the symbol  $\Phi$  means a dot product of the two unit vectors involved in the parenthesis (here are  $\mathbf{V}$  and  $\mathbf{N}$ ).  $\mathbf{N}$  is normal of the slip surface on which  $\mathbf{V}$  is developed. The energy dissipation developed on the slip surface can be determined by Eq.(14).

(2) The requirement for kinematical compatibility as expressed by the following equations enables the calculation of the velocity field,

$$\mathbf{V}_{i \leftrightarrow j} = \mathbf{V}_{i, j} - \mathbf{V}_{i, j-1}, \quad (40)$$

$$\mathbf{V}_{i \Downarrow j} = \mathbf{V}_{i, j} - \mathbf{V}_{i-1, j}. \quad (41)$$

The calculations start from the ‘neutral plane’ (Fig.20), which represents the main direction of sliding movement and is assumed to move without lateral component. Eqs.(40) and (41) allow a successive determination of  $\mathbf{V}_{i, j}$ . By substituting  $\mathbf{V}_{i, j}$  and  $D$  into Eq.(38), the factor of safety is obtained.

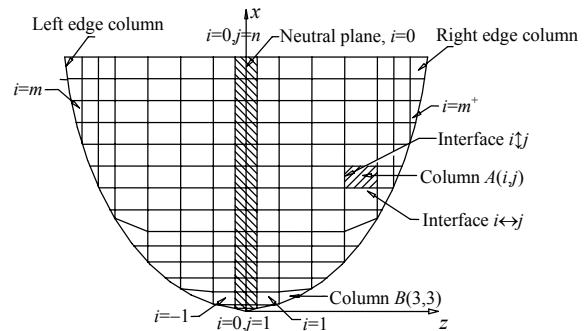


Fig.20 A plan view of the discretization pattern of the failure mass

### An illustrative examples

**Example 5** The testing problems presented by Zhang (1988)

The two examples presented by Zhang (1988) are shown in Fig.21. These problems have been re-evaluated by a number of authors as part of the validation process for their 3D analysis methods (Lam and Fredlund 1993; Huang and Tsai, 2000).

**Case 1** The ellipsoidal spherical slip surface

The slip surface has a circular shape at the central  $xoy$  plane and extends in the lateral  $z$  direction by elliptic lines. Chen *et al.*(2001a) reported the upper-bound solutions using the method described in

Section "The 3D upper-bound analysis".

They obtained a factor of safety of  $F=2.262$ . This can be compared with Zhang (1988)'s solution of  $F=2.122$ . Reanalysis using the limit equilibrium 3D Spencer method results in  $F=2.187$ . Fig.22 shows the isometric view of the failure mass.

**Case 2** The ellipsoidal spherical slip surface with a weak seam

This case concerns the ellipsoidal spherical slip surface that is partly replaced with a plane representing a weak seam, shown as Case 2 in Fig.23. This example, from (Zhang, 1988), has also been reevaluated by a number of authors, whose solutions are summarized in Table 1. The upper-bound and 3D Spencer solutions are 1.717 and 1.640 respectively.

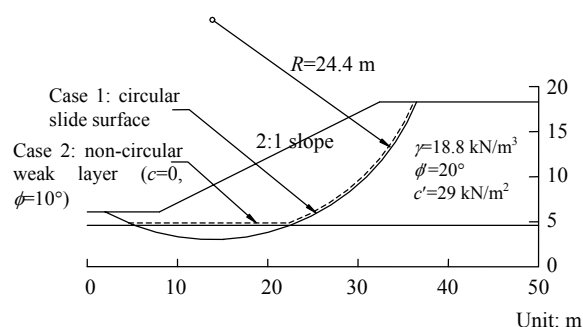


Fig.21 Zhang (1988)'s example. Case 1: an ellipsoid sphere slip surface; Case 2: the slip surface with a composite shape containing a weak plane

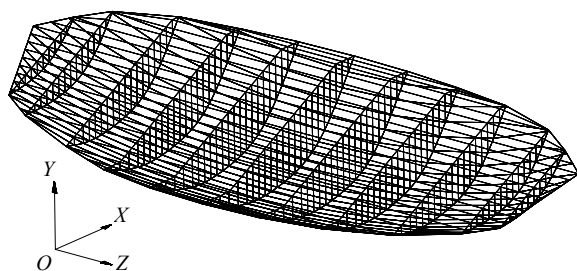


Fig.22 Case 1 of Example 5, an isometric view of the failure mass with vertical interfaces

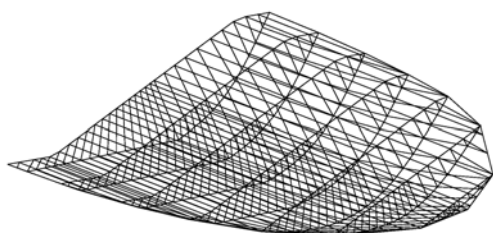


Fig.23 Case 2 of Example 5, an isometric view of the failure mass with a horizontal weak seam

**Table 1 Comparisons of the results from various authors for Zhang (1988)'s example, Case 2 in Fig.23**

Methods	Value
Zhang (1988)	1.553
Hungr <i>et al.</i> (1989)	1.620
Lam and Fredlund (1993)	1.603
Huang and Tsai (2000)	1.658
Chen <i>et al.</i> (2001a)'s upper-bound	1.717
Chen <i>et al.</i> (2003)'s limit equilibrium	1.640

## CONCLUSION

This paper provides the traditional soil mass stability analysis methods with a sound theoretical background based on Plasticity and endorses them a system of well organized mathematical formulations, in which a mature discipline of mechanics should have possessed. Main findings are summarized as follows:

(1) The solution of a slope stability analysis can be bracketed by its upper- and lower-bounds, provided by the limit analysis of Plasticity, i.e.  $F_{lower} < F_{real} < F_{upper}$ .

(2) The methods of vertical slices, referred to as generalized methods of slices, imply lower-bound solutions. It has been successfully extended to the area of active earth pressure analysis that accounts for different input of locations of earth pressure applications.

(3) The method of inclined interfaces gives an upper-bound approach to the stability analysis. It enjoys a sound mechanical background and is able to provide accurate solutions of soil plasticity. It has been successfully extended to the area of bearing capacity analysis in which various empirical coefficients are no longer necessary.

(4) The 3D upper- and lower-bound methods have been made possible and shown great potential for solving various engineering problems.

## References

- Bishop, A.W., 1955. The use of the slip circle in the stability analysis of slopes. *Geotechnique*, **5**(1):7-17.
- Chen, W.F., 1975. *Limit Analysis and Soil Plasticity*. Elsevier.
- Chen, Z., 1992. Random trials used in determining global minimum factors of safety of slopes. *Canadian Geotechnical Journal*, **29**(2):225-233.
- Chen, Z., Morgenstern, N.R., 1983. Extensions to the generalized method of slices for stability analysis. *Canadian Geotechnical Journal*, **20**(1):104-119.

- Chen, Z., Shao, C., 1988. Evaluation of minimum factor of safety in slope stability analysis. *Canadian Geotechnical Journal*, **25**(4):735-748.
- Chen, Z.Y., Li, S.M., 1998. Evaluation of active earth pressure by the generalized method of slices. *Canadian Geotechnical Journal*, **35**(4):591-599. [doi:10.1139/cgj-35-4-591]
- Chen, Z., Wang, X., Haberfield, C., Yin, J., Wang, Y.A., 2001a. Three-dimensional slope stability analysis method using the upper bound theorem, Part I: Theory and methods. *International Journal of Rock Mechanics and Mining Sciences*, **38**(3):369-378. [doi:10.1016/S1365-1609(01)00012-0]
- Chen, Z., Wang, J., Yin, J., Wang, J., Haberfield, C.A., 2001b. Three-dimensional slope stability analysis method using the upper bound theorem, Part II: Numerical approaches, applications and extensions. *International Journal of Rock Mechanics and Mining Sciences*, **38**(3):379-397. [doi:10.1016/S1365-1609(01)00013-2]
- Chen, Z., Mi, H., Zhang, F., Wang, X., 2003. A simplified method for 3D slope stability analysis. *Canadian Geotechnical Journal*, **40**(3):675-683. [doi:10.1139/t03-002]
- Chen, Z.Y., Wang, X.G., Yang, J., Jia, Z., Wang, Y.J., 2005. Rock Slope Stability Analysis: Theory, Method and Computer Programs. China Water Resources Press, Beijing (in Chinese).
- Donald, I.B., Giam, P., 1992. The ACADS Slope Stability Programs Review. Proc. 6th International Symposium on Landslides, **3**:1665-1670.
- Donald, I.B., Chen, Z.Y., 1997. Slope stability analysis by an upper bound plasticity method. *Canadian Geotechnical Journal*, **34**(6):853-862. [doi:10.1139/cgj-34-6-853]
- Duncan, J.M., 1996. State of the art: Limit equilibrium and finite element analysis of slopes. *ASCE Journal of Geotechnical Engineering*, **122**(7):577-596. [doi:10.1061/(ASCE)0733-9410(1996)122:7(577)]
- Huang, C.C., Tsai, C.C., 2000. New method for 3D and asymmetric slope stability analysis. *ASCE Journal of Geotechnical and Environmental Engineering*, **126**(10):917-927. [doi:10.1061/(ASCE)1090-0241(2000)126:10(917)]
- Hungr, O., Salgado, F.M., Byrne, P.M., 1989. Evaluation of a three dimensional method of slope stability analysis. *Canadian Geotechnical Journal*, **26**(4):679-686.
- Janbu, N., 1973. Slope Stability Computations. In: Hirschfield, E., Poulos, S. (Eds.), Embankment Dam Engineering, Casagrande Memorial Volume. John Wiley, New York, p.47-86.
- Lam, L., Fredlund, D.G., 1993. A general limit equilibrium model for three-dimensional slope stability analysis. *Canadian Geotechnical Journal*, **30**:905-919.
- Morgenstern, N.R., 1992. The Evaluation of Slope Stability—A 25 Year Perspective. Stability and Performance of Slopes and Embankments. ASCE Geotechnical Special Publications, p.1-26.
- Morgenstern, N.R., Price, V., 1965. The analysis of the stability of general slip surface. *Geotechnique*, **15**(1):79-93.
- Peck, R., 1990. Fifty Years of Lateral Earth Pressure. Proc. of Conf. on Design and Performance of Earth Retaining Structures. Cornell University, Ithaca, New York. ASCE Geotechnical Special Publication, No. 25.
- Sarma, K.S., 1979. Stability analysis of embankments and slopes. *J. Geotech. Am. Soc. Civ. Engrs.*, **105**(12):1511-1524.
- Seed, R.B., Mitchell, J.K., Seed, H.B., 1990. Kettleman Hills waste landfill slope failure, II: stability analysis. *ASCE Journal of Geotechnical Engineering*, **116**(4):669-690.
- Sokolovski, V.V., 1960. Statics of Soil Media (Translated by Jones D.H. and Scholfield A.N.). Butterworth, London.
- Spencer, E., 1967. A method of analysis of embankments assuming parallel inter-slice forces. *Geotechnique*, **17**:11-26.
- Wang, Y.J., Yin, J.H., Chen, Z.Y., 2001. Calculation of bearing capacity of a strip footing using an upper bound method. *International Journal for Numerical and Analytical Methods in Geomechanics*, **25**(8):841-851. [doi:10.1002/nag.151]
- Zhang, X., 1988. Three-dimensional stability analysis of concave slopes in plan view. *ASCE Journal of Geotechnical Engineering*, **114**(6):658-671.